

## Origin of the Diverse Melting Behaviors of Intermediate-Size Nanoclusters: Theoretical Study of $Al_N$ ( $N = 51-58, 64$ )

Joongoo Kang,<sup>\*,†</sup> Su-Huai Wei,<sup>†</sup> and Yong-Hyun Kim<sup>\*,‡</sup>

National Renewable Energy Laboratory, Golden, Colorado 80401, United States Graduate School of Nanoscience and Technology (WCU), KAIST, Daejeon 305-701, Korea

Received August 25, 2010; E-mail: Joongoo.Kang@nrel.gov (J.K.); Yong.Hyun.Kim@kaist.ac.kr (Y.-H.K.)

**Abstract:** Microscopic understanding of thermal behaviors of metal nanoparticles is important for nanoscale catalysis and thermal energy storage applications. However, it is a challenge to obtain a structural interpretation at the atomic level from measured thermodynamic quantities such as heat capacity. Using first-principles molecular dynamics simulations, we reproduce the size-sensitive heat capacities of  $Al_N$  clusters with  $N$  around 55, which exhibit several distinctive shapes associated with diverse melting behaviors of the clusters. We reveal a clear correlation of the diverse melting behaviors with cluster core symmetries. For the  $Al_N$  clusters with  $N = 51-58$  and 64, we identify several competing structures with widely different degree of symmetry. The conceptual link between the degree of symmetry (e.g.,  $T_d$ ,  $D_{2d}$ , and  $C_s$ ) and solidity of atomic clusters is quantitatively demonstrated through the analysis of the configuration entropy. The size-dependent, diverse melting behaviors of Al clusters originate from the reduced symmetry ( $T_d \rightarrow D_{2d} \rightarrow C_s$ ) with increasing the cluster size. In particular, the sudden drop of the melting temperature and appearance of the dip at  $N = 56$  are due to the  $T_d$ -to- $D_{2d}$  symmetry change, triggered by the surface saturation of the tetrahedral  $Al_{55}$  with the  $T_d$  symmetry.

### Introduction

Metal nanoclusters have been widely used for several emerging technologies because of their unique size-selective properties that are different from those of bulk materials. Recently, Al nanoclusters have been attracting much attention because many interesting phenomena have been reported for these nanoclusters.<sup>1-8</sup> For instance, recent experiments<sup>6</sup> showed that melting drastically enhances the catalytic reactivity of the chemisorption of  $N_2$  molecules on Al nanoclusters. Al nanoclusters also have size-selective reactivity for the dissociative chemisorption of water.<sup>4,5</sup> Not only the catalytic reactivity but also the melting of such nanoclusters is inherently size dependent.<sup>1-3,9-13</sup> From measurements of heat capacities,

Jarrold and co-workers<sup>1-3</sup> have elegantly demonstrated unusual diverse melting behaviors in size-selected Al nanoclusters with about 55 atoms. The  $Al_N$  clusters with  $N = 53-55$  have a single broadened, but clearly noticeable, peak in heat capacity (category I) with an almost constant peak position. The melting peak, which is centered at the melting temperature  $T_m$ , separates solidlike states and liquidlike states. As the cluster size  $N$  increases from 55 to 56, the melting point suddenly drops by 120 K, and at the same time a dip appears in the heat capacity just below the melting peak (category II). For a certain cluster such as  $Al_{64}$  and  $Al_{68}$ , there is no noticeable melting peak in the heat capacity (category III). The representative heat capacities are shown in Figure 1.

Despite great interest in Al nanoclusters and other metal clusters, a full atomic-level understanding of the observed phenomena is still lacking. Several simple phenomenological models<sup>2,3</sup> with some fitting parameters have been proposed to explain the observed heat capacities of Al clusters. Nonetheless, one needs atomistic interpretations to fully understand what actually happens during the melting processes. Previous molecular dynamics (MD) simulations using Gupta<sup>14,15</sup> and glue<sup>14</sup> empirical potentials failed to reproduce the melting features of the measured heat capacities of intermediate-size Al nanoclusters with about 55 atoms. This discrepancy indicates that more accurate interatomic potentials are necessary to describe the nanoscale melting of the intermediate-size Al clusters. More

\* To whom correspondence should be addressed.

† National Renewable Energy Laboratory.

‡ Graduate School of Nanoscience and Technology (WCU), KAIST.

- (1) Breaux, G. A.; Neal, C. M.; Cao, B.; Jarrold, M. F. *Phys. Rev. Lett.* **2005**, *94*, 173401.
- (2) Neal, C. M.; Starace, A. K.; Jarrold, M. F. *Phys. Rev. B* **2007**, *76*, 054113.
- (3) Jarrold, M. F.; Cao, B.; Starace, A. K.; Neal, C. M.; Judd, O. H. *J. Chem. Phys.* **2008**, *129*, 014503.
- (4) Roach, P. J.; Woodward, W. H.; Castleman, A. W., Jr.; Reber, A. C.; Khanna, S. N. *Science* **2009**, *323*, 492.
- (5) Shimojo, F.; Ohmura, S.; Kalia, R. K.; Nakano, A.; Vashishta, P. *Phys. Rev. Lett.* **2010**, *104*, 126102.
- (6) Cao, B.; Starace, A. K.; Judd, O. H.; Jarrold, M. F. *J. Am. Chem. Soc.* **2009**, *131*, 2446.
- (7) Xiang, H.; Kang, J.; Wei, S.-H.; Kim, Y.-H.; Curtis, C.; Blake, D. *J. Am. Chem. Soc.* **2009**, *131*, 8522.
- (8) Kang, J.; Kim, Y.-H. *ACS Nano* **2010**, *4*, 1092.
- (9) Labastie, P.; Whetten, R. L. *Phys. Rev. Lett.* **1990**, *65*, 1567.
- (10) Schmidt, M.; Kusche, R.; v. Issendorff, B.; Haberland, H. *Nature* **1998**, *393*, 238.
- (11) Schmidt, M.; Donges, J.; Hippler, Th.; Haberland, H. *Phys. Rev. Lett.* **2003**, *90*, 103401.

- (12) Haberland, H.; Hippler, Th.; Donges, J.; Kostko, O.; Schmidt, M. v.; Issendorff, B. *Phys. Rev. Lett.* **2005**, *94*, 035701.
- (13) Starace, A. K.; Neal, C. M.; Cao, B.; Jarrold, M. F.; Aguado, A.; López, J. M. *J. Chem. Phys.* **2008**, *129*, 144702.
- (14) Noya, E. G.; Doye, J. P. K.; Calvo, F. *Phys. Rev. B* **2006**, *73*, 125407.
- (15) Zhang, W.; Zhang, F.; Zhu, Z. *Phys. Rev. B* **2006**, *74*, 033412.

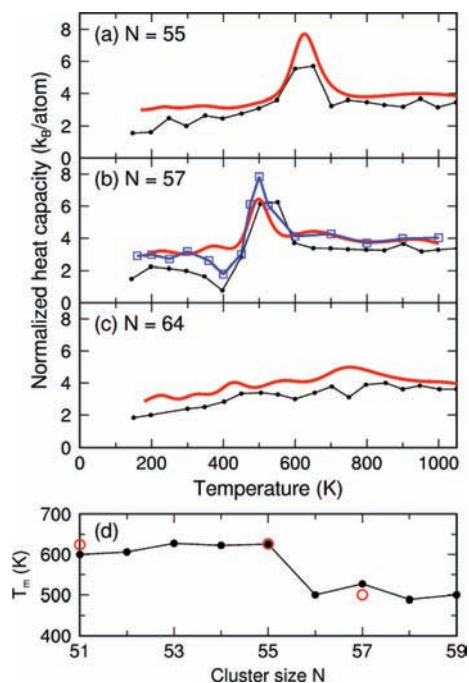


**Figure 1.** (a–c) Simulated heat capacity (red line) from MD simulations is compared with experimental data (black dot and line) taken from refs 1 and 2 for  $Al_N$  clusters with  $N = 55, 57,$  and  $64,$  respectively. In (b) for  $N = 57,$  we also present the simulated heat capacity  $C(T_i)$  at temperatures  $T_i$  (blue square and line), including the freezing effect below  $T_{dip}$  (text). The continuous heat capacity under the equilibrium condition was calculated from the multiple-histogram method,<sup>18</sup> while the discrete heat capacity  $C(T_i)$  under the nonequilibrium condition was obtained from averaged-energy ensembles  $E(T_i)$  and the finite difference method. In (d), the measured melting points of Al clusters (black dot, taken from ref 1) are shown with the simulated points of  $Al_{51}, Al_{55},$  and  $Al_{57}$  (red open circles).

recently, using the state-of-the-art NP-B empirical potentials,<sup>16</sup> Li and Truhlar<sup>17</sup> performed comprehensive MD simulations of size-selected Al clusters and provided new insight into the character of cluster nanophases. However, fully quantum mechanical calculations of melting of Al nanoclusters have been mainly limited to very small clusters like  $Al_{13}$  (ref 18) due to high computational cost.

Only recently, the melting of the  $Al_{55}$  cluster was studied using first-principles molecular dynamics simulations, which showed unusual tetrahedral-like  $Al_{55}$  clusters and their novel, collective surface melting behaviors.<sup>8</sup> Although the tetrahedral-like  $Al_{55}$  cluster has the surface atoms at the corners with a low coordination number of four, it is much more stable than the more spherical (of least surface area) icosahedral 55 atom cluster by 4.8 eV from the density functional theory (DFT) calculations.<sup>8</sup> The tetrahedral-like  $Al_{55}$  cluster was also supported from photoelectron spectrum.<sup>8</sup> For other elements, Ga and In, with the same  $s^2p^1$  electron configuration as Al, the tetrahedral-like structure is energetically more favorable than the icosahedral structure by 3.2 and 1.3 eV, respectively. By contrast, other metallic clusters with the valence electrons mostly derived from atomic s orbitals – such as Na ( $3s^1$ ), Cu ( $3d^{10}4s^1$ ), and Ag ( $4d^{10}5s^1$ ) – have the icosahedral ground state for 55 atom

systems,<sup>19</sup> which is more stable than the tetrahedral state by 2.0, 5.5, and 3.6 eV, respectively. Unlike in the case of the s orbital systems, the hybridization between s and p orbitals of the  $Al(3s^23p^1)$  clusters can effectively stabilize the low-coordination surface atoms. As a result, the Al clusters can have several energetically competitive structures, which include low-coordination surface atoms. We will show later that the structural diversity ultimately leads to the diverse and size-sensitive melting behaviors of Al clusters.

In this article, we address the fundamental issues regarding the melting of Al nanoclusters from first-principles molecular dynamics (MD) simulations and advanced statistical analysis. First, we demonstrate that the diverse melting behaviors of Al clusters (categories I to III) can be captured through the analysis of the calculated configuration entropy. Next, we show that the change of melting behavior of  $Al_N$  clusters from category I to III, including a sudden drop of  $T_m$  at  $N = 56,$  can be understood by the reduced cluster symmetry ( $T_d \rightarrow D_{2d} \rightarrow C_s$ ) as the cluster size  $N$  increases from 55 to 56 and to 64. The saturated tetrahedral  $Al_{55}$  cluster with a  $T_d$   $Al_{10}$ -core serves as a boundary marking the abrupt change in melting behaviors.

## Computational Methods

In this study, total energies of Al clusters were calculated within the generalized gradient approximation (GGA-PBE<sup>20</sup>) to the density functional theory (DFT) as implemented in the VASP package<sup>21,22</sup> using projector-augmented wave potentials.<sup>23</sup> First-principles MD simulations were performed with the Nosé thermostat<sup>24</sup> at simulation temperatures ranging from 130 to 1200 K, and the time step was chosen to be 3 fs. We calculated heat capacities of representative clusters,  $Al_{51}, Al_{55}, Al_{57},$  and  $Al_{64},$  using the well-established multiple-histogram method.<sup>8,9,18</sup> The total sampling times for equilibrium ensembles were 5.7, 5.3, 5.8, and 4.1 ns for  $N = 51, 55, 57,$  and  $64,$  respectively. To reduce computing time of the energy samplings, we used nonspin-polarized DFT calculations for the extensive first-principles MD simulations. We found that the energy correction after spin-polarized calculations is only a few 10 meV for the intermediate-size Al clusters. Thus, the spin-polarization effect is insignificant compared to the large thermal energy fluctuations in the MD simulations. The calculated melting temperatures are in excellent agreement with the measured values (Figure 1 and Figure S1 in the Supporting Information).

## Results and Discussion

To study melting of  $Al_N$  clusters, we first need to know their ground-state structures. As an unbiased method with no assumption regarding cluster geometry, first-principles MD simulations were employed using high-energy structures as an initial state. We found that a long-run MD simulation (up to 1 ns) at a constant temperature around  $0.8\text{--}0.9 T_m$  within a broadened melting peak is an efficient way to search ground- or near-ground-state structures for intermediate-size Al clusters containing more than 50 atoms.<sup>8</sup> Some of the identified geometries share similar structural motifs with the recently proposed geometries<sup>13</sup> that were generated from decahedral fragments and their variations (Supporting Information). To validate whether

(16) Jasper, A. W.; Schultz, N. E.; Truhlar, D. G. *J. Phys. Chem. B* **2005**, *109*, 3915.

(17) Li, Z. H.; Truhlar, D. G. *J. Am. Chem. Soc.* **2008**, *130*, 12698.

(18) Chandrachud, P.; Joshi, K.; Kanhere, D. G. *Phys. Rev. B* **2007**, *76*, 235423.

(19) Häkkinen, H.; Moseler, M.; Kostko, O.; Morgner, N.; Hoffmann, M. A.; v. Issendorff, B. *Phys. Rev. Lett.* **2004**, *93*, 093401.

(20) Perdew, J. P.; Burke, K.; Ernzerhof, M. *Phys. Rev. Lett.* **1996**, *77*, 3865.

(21) Kresse, G.; Furthmüller, J. *Phys. Rev. B* **1996**, *54*, 11169.

(22) Kresse, G.; Joubert, D. *Phys. Rev. B* **1999**, *59*, 1758.

(23) Blöchl, P. E. *Phys. Rev. B* **1994**, *50*, 17953.

(24) Nosé, S. *J. Chem. Phys.* **1984**, *81*, 511.

(25) Wales, D. J.; Doye, J. P. K. *J. Phys. Chem. A* **1997**, *101*, 5111.

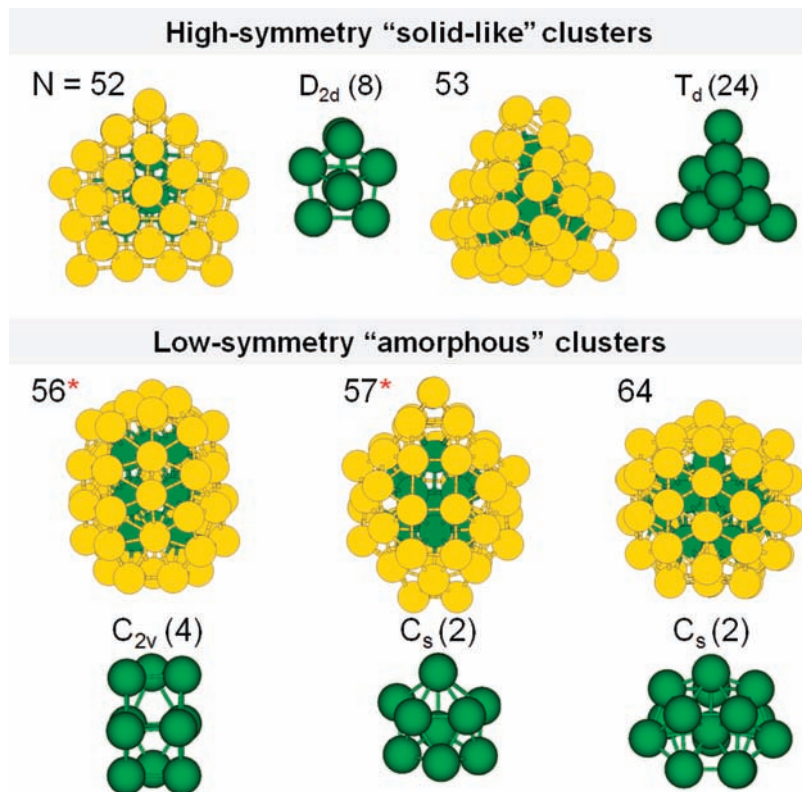
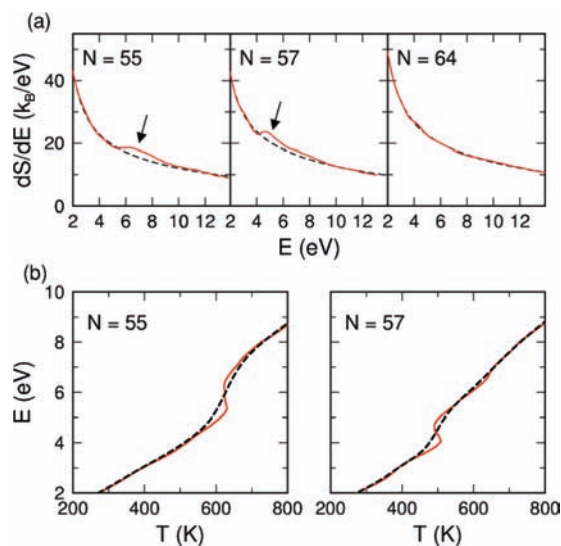


**Figure 2.** Classification of low-energy Al nanoclusters with about 55 atoms. The Al atoms in the core region are colored green, while the atoms on the surface are colored yellow. The core cluster is also displayed for each  $Al_N$  cluster. The number in parentheses is a number of symmetry operations. For  $N = 56^*$  and  $57^*$ , we present metastable low-symmetry geometries. The lowest-energy geometries of  $Al_{56}$  and  $Al_{57}$  can be found in Figure 4.

the identified structures are ground-state structures, we also conducted systematic global optimizations of  $Al_{55}$  and  $Al_{57}$  using the Monte Carlo basin-hopping method<sup>25,26</sup> within the DFT. Among newly identified 30 000 (22 000) local minima for  $Al_{55}$  ( $Al_{57}$ ), we could locate a group of low-energy structures that have the nearly same geometries as the lowest-energy clusters obtained from the MD simulations, apart from some excited surface atoms (Supporting Information).

From the MD simulations in neutral charge state, we identified several low-energy geometries of  $Al_N$  clusters with  $N = 51-58$  and 64 (Figure 2 and Figure S2 in the Supporting Information). The intermediate-size clusters have a well-defined core and surface. We found that all the low-energy geometries can be classified based on the symmetry of the core region as (i) tetrahedron ( $T_d$ ), (ii) bidisphenoid ( $D_{2d}$ ), and (iii) low-symmetry cores ( $C_{2v}$  or  $C_s$ ). For instance, the neutral clusters with  $N = 53-55$  adopt the  $T_d$   $Al_{10}$ -core geometries as their lowest-energy structures. In contrast, the clusters with  $N = 50-52$ , 56, and 57 have the bidisphenoid  $Al_8$  ( $D_{2d}$ ) as the common core.  $Al_{64}$  is a low-symmetry cluster with only one reflection symmetry ( $C_s$ ). In addition, we identified several low-energy metastable structures,  $Al_{56}^*$  and  $Al_{57}^*$  (Figure 2), that have lower symmetry than the ground-state structures. We will show later that the presence of the low-symmetry metastable structures is crucial to account for the melting behavior in category II.

The classification of Al clusters based on symmetry reveals a clear correlation between the stability of the clusters and the point group symmetry. The lowest-energy Al clusters generally have relatively high symmetry such as  $T_d$  and  $D_{2d}$ , as compared

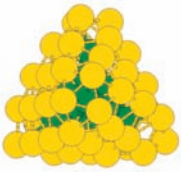
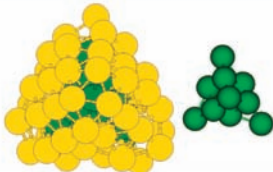
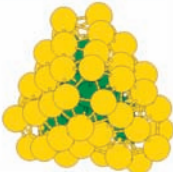
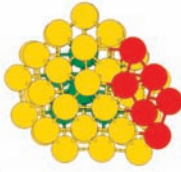
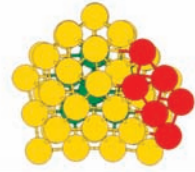
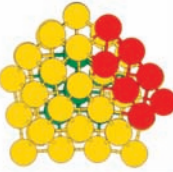


**Figure 3.** (a) The calculated first-order energy derivative of the configuration entropy ( $dS/dE$ , solid lines) of  $Al_N$  clusters with  $N = 55, 57$ , and 64. The energy zero is the one for the lowest-energy structure for a given cluster size. Dashed lines are given for guidance of eyes. (b) The calculated caloric curves of  $Al_{55}$  and  $Al_{57}$  for microcanonical results (red solid lines) and canonical results (black dashed lines). The microcanonical caloric curve was obtained from the relation,  $1/T = \partial S/\partial E$ , for the microcanonical temperature  $T$ , entropy  $S$ , and energy  $E$ .

to the metastable, low-symmetry clusters. By contrast, the icosahedral-like Al clusters are relatively unstable despite their high approximate point-group symmetry ( $I_h$ ) (Supporting Information). This trend can be understood from the principle of maximum symmetry, which explains why clusters with higher symmetry (e.g.,  $T_d$ ,  $D_{2d}$ , and  $I_h$ ) are more likely to be particularly

(26) Wales, D. J.; Scheraga, H. A. *Science* **1999**, 285, 1368.

(27) Wales, D. J. *Chem. Phys. Lett.* **1998**, 285, 330.

Size N	55	56	57
$T_d$			
$D_{2d}$			
$\Delta(\text{eV})$	-0.35	0.005	0.24

**Figure 4.** Structural change from  $T_d$  to  $D_{2d}$  clusters with increasing cluster size. For each size  $N$ , the most stable clusters based on the  $T_d$   $\text{Al}_{10}$  and  $D_{2d}$   $\text{Al}_8$  cores are listed. The relative stability ( $\Delta$ ),  $\Delta = E(T_d) - E(D_{2d})$ , is also shown. The Al atoms in the core region are colored green, while the atoms on the surface are colored yellow. For  $N = 56$ , core regions are also displayed to show the large distortion of the  $T_d$   $\text{Al}_{10}$  core. For  $\text{Al}_{55}$  ( $D_{2d}$ ), three of the four corner atoms of the  $\text{Al}_{52}$  ( $D_{2d}$ ) in Figure 2 are cut and transferred to the outer empty shell to form the six-atom cluster (red balls) with the three added atoms. Likewise, only two corner atoms of the  $\text{Al}_{52}$  are removed to form  $\text{Al}_{56}$  and  $\text{Al}_{57}$  with the  $D_{2d}$  symmetry.

low- and high-energy minima.<sup>27</sup> At finite temperature, however, a low-symmetry state may have the lowest free energy due to entropy effect.<sup>28</sup>

The degree of cluster symmetry manifests itself in the variation of the configuration entropy and thus the cluster melting. Configuration entropy ( $S$ ) is an important quantity for thermodynamics, which, once known, enables us to calculate all other thermodynamic functions and properties.<sup>9</sup> Here,  $S = k_B \ln \Omega(E)$ , where  $\Omega(E)$  is a density of accessible configurations at energy  $E$  in potential energy surface, and  $k_B$  is the Boltzmann constant. A previous theoretical work<sup>29</sup> calculated configuration entropy and partition function of Al clusters to determine free energy of nanocluster formation. To show how configuration entropy relates to cluster symmetry, we calculated the configuration entropy and heat capacities of three representative Al clusters,  $\text{Al}_{55}$  ( $T_d$ ),  $\text{Al}_{57}$  ( $D_{2d}$ ), and  $\text{Al}_{64}$  ( $C_s$ ), using the multiple-histogram method.<sup>18</sup> Part a of Figure 3 shows the first-order energy derivative of the configuration entropy ( $dS/dE$ ) as a function of energy. The high-symmetry clusters, such as  $\text{Al}_{55}$  and  $\text{Al}_{57}$ , have a bump (as indicated by arrows) in the  $dS/dE$  plot. This is because the atoms of the high-symmetry cluster find it energetically more favorable to maintain certain fixed positional relationships with each other. Hence, for energy below a certain threshold, the cluster symmetry is more or less preserved. This leads to a solidity or rigidity of the high-symmetry cluster, in analogy with the corresponding emergent property of bulk solid. The high degree of symmetry is only broken catastrophically above the threshold energy, leading to the abrupt increase of  $\Omega$  and the bump in the  $dS/dE$  plot. Consequently, the high-symmetry cluster exhibits a sharp heat capacity peak, which separates the solidlike and liquidlike states (Figure 1). On the other hand, the low-symmetry  $\text{Al}_{64}$  does not have the solidity of  $\text{Al}_{55}$  and  $\text{Al}_{57}$ . Thus, the  $dS/dE$  plot is featureless (part a of Figure 3) and so is the heat capacity (Figure 1).

The first-order-like melting transition of  $\text{Al}_{55}$  and  $\text{Al}_{57}$  is characterized by the dynamic coexistence<sup>9,17,30–35</sup> of solidlike and liquidlike states. Near  $T_m$ , a cluster can repetitively switch back and forth between solidlike states and liquidlike states. Unlike in bulk materials, the phase separation of the two states is highly improbable for such small clusters due to large interface energy. The relative probability of finding a cluster in the solidlike (or liquidlike) states is thermodynamically given by the so-called two-state model,<sup>34,35</sup> which also relates  $T_m$  with the energy difference and the entropy difference between the solidlike and liquidlike regions of the configuration space. Part b of Figure 3 shows an S-bend in the microcanonical caloric curve near  $T_m$ , which is a thermodynamic signature of the dynamic coexistence.<sup>9,33–35</sup>

Simulated heat capacities of the  $\text{Al}_{55}$  and  $\text{Al}_{64}$  agree well with the experimental results (Figure 1). For the  $\text{Al}_{57}$ , however, there is qualitative inconsistency: the simulated heat capacity has a simple melting peak at  $T_m = 500$  K, while a dip appears in the measured heat capacity at  $T_{\text{dip}} = 400$  K, just below the  $T_m$  (ref 1). We find that this discrepancy is closely related to different procedures in simulating and measuring heat capacities. In the simulation, we first performed a MD simulation at a constant temperature  $T = 400$  K ( $0.8 T_m$ ), starting from high-energy states, until the lowest-energy  $\text{Al}_{57}$  ( $D_{2d}$ ) cluster emerged after 180 ps (Figure 4). From a separate MD simulation at the elevated temperature  $T = 450$  K ( $0.9 T_m$ ), we obtained the same geometry in a shorter simulation time (150 ps). Then, the low- $T$  energy ensembles below 400 K were obtained from MD simulations with the ground-state cluster as an initial geometry. By contrast, in experiments, the cluster energy,  $E(T)$ , is measured *independently* at each temperature: the Al cluster, which is prepared at extremely high temperature, is thermalized at a given low temperature before its energy is measured. Our simulations show that at sufficiently high temperature ( $T =$

(28) Li, Z. H.; Jasper, A. W.; Truhlar, D. G. *J. Am. Chem. Soc.* **2007**, *129*, 14899.

(29) Li, Z. H.; Bhatt, D.; Schultz, N. E.; Siepmann, J. I.; Truhlar, D. G. *J. Phys. Chem. C* **2007**, *111*, 16227.

(30) Wales, D. J.; Berry, R. S. *J. Chem. Phys.* **1990**, *92*, 4283.

(31) Matsuoka, H.; Hirokawa, T.; Matsui, M.; Doyama, M. *Phys. Rev. Lett.* **1992**, *69*, 297.

(32) Kunz, R. E.; Berry, R. S. *Phys. Rev. Lett.* **1993**, *71*, 3987.

(33) Wales, D. J.; Berry, R. S. *Phys. Rev. Lett.* **1994**, *73*, 2875.

(34) Doye, J. P. K.; Wales, D. J. *J. Chem. Phys.* **1995**, *102*, 9673.

(35) Wales, D. J.; Doye, J. P. K. *J. Chem. Phys.* **1995**, *103*, 3061.

0.8–0.9  $T_m$ ), the ground-state structure can easily emerge within a nanosecond during the thermalization. At low temperature, however, the cluster may freeze to high-energy geometries due to the rapid, stepwise quenching, which can lead to a dip in the heat capacity.<sup>3</sup> To check this idea, we performed a MD simulation at  $T = 360$  K (0.7  $T_m$ ) as we did to find the lowest-energy  $Al_{57}$  at  $T = 400$  and 450 K. In this case, within the simulation time, the cluster was stabilized to a metastable low-symmetry  $Al_{57}^*$  ( $C_s$ ) structure shown in Figure 2. At zero temperature, the  $Al_{57}^*(C_s)$  is less stable than the  $Al_{57}(D_{2d})$  by  $\Delta E = 0.45$  eV. As another example in category II, we identified a metastable low-symmetry  $Al_{56}^*$  ( $C_{2v}$ ) with  $\Delta E = 0.19$  eV through MD simulation at 320 K over 1.05 ns (Figure 2). By employing the metastable  $Al_{57}^*$  as an initial geometry to obtain the ensemble-averaged energies,  $E(T)$ , for low temperatures below  $T_{dip} = 400$  K, we succeeded in reproducing the dip of the measured heat capacity (Figure 1). This indicates that the dip appears due to the freezing effect below the  $T_{dip}$ .

Finally, we demonstrate that two plateaus of melting point ( $T_m$ ) at  $N = 53-55$  and  $56-58$  and a sudden drop of  $T_m$  at  $N = 56$  (Figure 1) can be understood by the structural transitions and competitions between clusters with different symmetries:

**$D_{2d}$  to  $T_d$  transition.** The  $D_{2d}$   $Al_8$ -core clusters are the ground states for neutral clusters with  $N = 50-52, 56$ , and 57. Among these clusters, the  $Al_{52}$  has the saturated (or fully occupied) surface shell with the  $D_{2d}$  symmetry (Figure 2). Hence, the added atom to the  $Al_{52}(D_{2d})$  should occupy the outer empty shell, which makes the  $Al_{53}$  energetically unfavorable to the tetrahedral isomer. Thus, the first structural change from  $D_{2d}$  to  $T_d$  cluster occurs as the cluster size increases from  $N = 52$  to 53.

**$T_d$  to  $D_{2d}$  transition.** For  $N = 53, 54$ , and 55, the tetrahedral-like Al clusters are the ground-state structures. They have  $T_d$   $Al_{10}$  as the common core with nearly identical surface atomic configurations: as  $N$  increases from 53 to 55, Al atoms are just added to the corner sites (Figures 2 and 4). Because of this structural similarity, the tetrahedral-like  $Al_{53}, Al_{54}$ , and  $Al_{55}$  should have similar configuration entropies and thus almost constant  $T_m$  at  $N = 53-55$ . We found that the surface of the  $T_d$   $Al_{10}$ -core structure becomes saturated at  $N = 55$ . When one atom is added to the fully occupied  $Al_{55}$ , the original  $T_d$  core gets largely distorted to accommodate the added atom to the saturated surface, as shown in Figure 4. Because of the large strain of the  $Al_{56}(T_d)$ , the relative stability of the  $T_d$  cluster compared to the  $D_{2d}$  cluster decreases from 0.35 eV to nearly zero as the size  $N$  increases from 55 to 56. Hence, the  $D_{2d}$ -core clusters shown in Figure 4, which are structurally very similar, become the ground-state geometries for  $N = 56-58$ , leading to the second plateau of  $T_m$  at around 500 K.

The  $T_d$ -to- $D_{2d}$  symmetry change, triggered by the surface saturation of the tetrahedral  $Al_{55}$ , explains the abrupt change in melting behaviors at the edge of the upper and lower plateaus. Considering the structural similarity between the metastable  $Al_{55}$

with the  $D_{2d}$  symmetry and the other  $D_{2d}$  clusters at the lower plateau (Figure 4), the metastable  $Al_{55}(D_{2d})$  should have a similar  $T_m$  to the lower plateau temperature. However, the high-symmetry, ground-state  $Al_{55}(T_d)$  is more stable than the  $Al_{55}(D_{2d})$  by 0.35 eV (6.4 meV/atom), which can be roughly translated to an increase of  $T_m$  by 74 K. As a result, the  $T_m$  of the  $Al_{55}(T_d)$  should be substantially higher than that of the  $Al_{56}$ , consistent with the abrupt drop of  $T_m$  at  $N = 56$  (Figure 1). At the same time, as the cluster symmetry is lowered from  $T_d$  to  $D_{2d}$ , another metastable  $Al_{56}^*$  with lower symmetry  $C_{2v}$  becomes energetically competitive with high-symmetry clusters ( $\Delta E = 0.19$  eV). Thus, the low-symmetry, metastable  $Al_{56}^*$  may act as a frozen state during a stepwise quenching at low temperature, and a dip can appear just below the  $T_m$  in the heat capacity (category II).

## Conclusions

In conclusion, our first-principles MD simulations show that the diverse melting behaviors of the intermediate-size  $Al_N$  clusters with  $N$  around 55 (categories I to III) can be understood by the competition between clusters with different degree of symmetry ranging from  $T_d$  to  $C_s$ . In particular, the symmetry change from  $T_d$  to  $D_{2d}$  due to the surface saturation effect explains the abrupt  $T_m$  drop at  $N = 56$  and the emergence of the dip in heat capacity. The methods used here can be generally applied to nanoclusters of other elements and sizes. We believe that the insights obtained in this study should be useful for understanding melting of other nanoclusters that can have a variety of structures for similar cluster sizes.

**Acknowledgment.** This work was funded by the U.S. DOE EERE CSP and NREL LDRD programs under Contract No. DE-AC36-08GO28308. This research used resources of the National Energy Research Scientific Computing Center, which is supported by the Office of Science of the U.S. Department of Energy under Contract No. DE-AC02-05CH11231. This research also used capabilities of the National Renewable Energy Laboratory Computational Sciences Center, which is supported by the Office of Energy Efficiency and Renewable Energy of the U.S. Department of Energy under Contract No. DE-AC36-08GO28308. Y.-H. Kim was also supported by WCU (World Class University) program through the National Research Foundation of Korea funded by the Ministry of Education, Science and Technology (R31-2008-000-10071-0). We thank A. K. Starace for discussions and for reading the manuscript.

**Supporting Information Available:** Structures and relative energies of the ground-state  $Al_N$  isomers for  $N = 51-58, 64$  are compared with the previous results from refs 13 and 25. This material is available free of charge via the Internet at <http://pubs.acs.org>.

JA107683M